JOURNAL OF SPACECRAFT AND ROCKETS
Vol. 36, No. 2, March–April 1999

Grooves Effect on Lift: Data Correlation and Prediction for Kinetic Energy Projectiles

Ameer G. Mikhail*
U.S. Army Research Laboratory, Aberdeen Proving Ground, Maryland 21005-5066

Effect of grooves on the normal force of an antiarmor long rod kinetic energy (KE) projectile is analyzed and numerically quantified. The effect was studied for body-alone and body with fins, where clear and distinct effects were experimentally observed for each. Wind-tunnel data sets were analyzed, and algebraic, semiempirical correlations were constructed utilizing the main physical parameters of the projectile body and fins, as well as the flow parameters. The correlations provide a simple method to estimate the increase or decrease in the vehicle total normal force due to grooves and can be implemented in fast aerodynamics design codes. One separate set of data was dedicated for independent validation, and the correlation predicted the effect well, both in magnitude and sign. The present correlation is the only one known for predicting the lift loss (or gain) due to grooves. In addition, a better understanding of the contributions of grooves to both body-alone and fins-in-presence-of-body is presented. The correlation is constructed for the Mach number range of 2.0 < M < 5.5 and small angles of attack of less than 6 deg, which cover the flight envelope of tactical KE antiarmor projectiles. The established correlations provide direct incremental corrections over smooth-body values, for useful direct design use.

Nomenclature

A_{ref} = reference area ($\pi d^2/4$), in.^{2}
CD = drag coefficient, drag force/($q_\infty A_{\text{ref}}$)
CL = lift coefficient, lift force/($q_\infty A_{\text{ref}}$)
CN = normal force coefficient, normal force/($q_\infty A_{\text{ref}}$)
CN_α = normal force slope coefficient, $\partial C_N/\partial\alpha$, rad^{-1}
d = projectile reference diameter, in.
G/G = grooved first body length/grooved second length
G/S = grooved first body length/smooth second length
G/T = grooved first body length/threaded second length
$K_{b(w)}$ = wing-body normal force interference modeling factor for a body in the presence of a wing
$K_{w(b)}$ = wing-body normal force interference modeling factor for a wing in the presence of a body
L = total length of the projectile, in.
l_g = length of grooved portion of the body, in.
l_{g1}, l_{g2} = lengths of grooved body portions if more than one existed, in.
M = Mach number of the projectile
N = number of fins in a fin set
p_1, p_2 = groove pitch, 1/(number of grooves per inch), in.
q_∞ = dynamic pressure, ($0.5\rho V^2$), psi
Re = flow Reynolds number per foot, ft^{-1}
R_∞ = Reynolds number based on projectile total length
V = projectile velocity, ft/s
α = body pitching angle of attack, deg
ρ = air density, slug/ft^3

Subscripts

b = body-alone, i.e., without fins
bf = body and fins
bfl = body and flare
f = fins, tail fins or wing fins
fl = flare
g = with body surface grooves
s = smooth-body surface, i.e., without grooves

Presented as Paper 98-0671 at the AIAA 36th Aerospace Sciences Meeting, Reno, NV, Jan. 12–15, 1998; received May 8, 1998; revision received Aug. 22, 1998; accepted for publication Aug. 27, 1998. This paper is declared a work of the U.S. Government and is not subject to copyright protection in the United States.

*Aerospace Engineer, Ballistics and Weapons Concepts Division, Weapons Technology and Materials Research Directorate. Associate Fellow AIAA.

Introduction

IN many instances in the design and testing of antiarmor kinetic energy (KE) projectiles, as the one shown in Fig. 1, the fin effectiveness in providing the normal force for stability and pitch damping is questioned due to the still nonquantified effect of the grooves of the rod body. These grooves are needed for the transmission of the launching force from the driving sabot. As for any other unquantified effect, this effect is usually either minimized or exaggerated. No prediction tool that can predict this generally small effect exists. In fact, it is generally not known if the grooves will increase or decrease the total vehicle lift force. Although generally acknowledged as small, one needs a fast prediction method to estimate the magnitude and the sign of the expected change in the normal force. This need is the motivating force behind the present work. The physical phenomenon of the grooves/boundary-layer interaction on the body and along the fin–body junction is not very simple and does not lend itself to fast prediction methods. The practical approach of relying on actual force measurements data and reading them back into empirically formulated expressions seems appealing and more practical. The same approach was used, a decade earlier by Mikhail,[1] in studying the effect of the grooves on the drag force. The grooves effect on the drag force is more pronounced than those on the lift force. Although empirical, those drag correlations were applied by other researchers[2] and were found to be very useful and more accurate[2] than other estimates.

The available data are relatively sparse, but sufficient to construct a correlation. Khan and Chung[3] wind-tunnel tested a body-alone with and without grooves. Brandon and von Wahlde[4] performed large-scale wind-tunnel tests of KE projectiles, including body-alone and body with fins. Sigal[5] tested body-alone and body with fins and with flare in wind tunnel but for limited Mach numbers. Fellows and Carberry[6] performed wind-tunnel tests for body with fins, which were later also reported by Hendry.[7]

Range tests were also performed on some limited configurations.[2,8] Because the groove effects are usually small, their effects usually fall close to the measurement accuracy of the normal force. In Ref. 8, few measuring stations were used and CN_α could not be reliably reduced from the data. Thus, no reliable values were available from free-flight range tests for grooved vs smooth models. Also, another range test was performed[9] with the same outcome regarding the uncertainty of the normal force slope coefficient measurements.

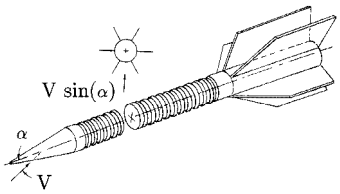

Fig. 1 Grooves of the typical KE projectile.

Hopefully, future firings may be aimed to obtaining more confirmed measurements.

The boundary layer over the grooved body section at the Mach number range of interest ($M = 2$–5) is always turbulent, except perhaps over the nose tip section. For a body-alone, the grooves seem to increase the pressure difference between the windward and leeward sides, causing an increase in the lift force. For finned bodies, the exact mechanisms affecting the fins are not very well explained. However, explanations are usually proposed that the grooves may increase the boundary-layer thickness or cause flow unsteadiness over the fins.

More recently, turbulent boundary-layer measurements were made[10] at Mach = 5 and zero angle of attack, for a flared body. Large grooves of square profiles of depths of 0.197 and 0.394 in. (for pitch of 2.54 and 1.27 grooves/in., respectively) and 45-deg saw-toothed grooves were tested. Surface pressure, turbulent boundary-layer parameters and heat flux measurements were reported. Because of the large groove pitch and depth, each single groove acts as a single cavity, where the flow impacts the facing surface of the circumferential cavity. Only flow variables, but no forces, were reported at the zero-angle-of-attack tests. The surface pressure was then integrated to estimate the forebody drag coefficient.

The purpose of this paper is to provide a fast predictive method to estimate the incremental fin lift force loss and the body lift force gain due to surface grooves, as a fraction of the corresponding smooth-body lift force value. This incremental value can then be used to correct the actual lift force.

Analysis

The effect of the grooves on the normal force is modeled as a correction factor to the normal force coefficient for the smooth-body value. Because we are dealing usually with small α, the lift force will be interchanged with the normal force without loss in meaning ($CN = CL\cos\alpha + CD\sin\alpha$, and for small α, $CN \approx CL$). First, the normal force for body–fin combination is usually written as

$$CN_{\alpha,bf} = CN_{\alpha,b} + \left(K_{w(b)} + K_{b(w)}\right)CN_{\alpha,ff} \tag{1}$$

$$\equiv CN_{\alpha,b} + CN_{\alpha,f} \tag{2}$$

where $CN_{\alpha,ff}$ is the pure fin-alone normal force with no body attached to it. Now, for body-alone we introduce the definition of F_b as

$$F_b = \frac{\Delta CN_{\alpha,b}}{CN_{\alpha,bs}} \equiv \frac{(CN_{\alpha,bg} - CN_{\alpha,bs})}{CN_{\alpha,bs}} \tag{3}$$

For body with fins, we introduce the factor F_{bf} as

$$F_{bf} = \frac{\Delta CN_{\alpha,bf}}{CN_{\alpha,bf,s}} \equiv \frac{(CN_{\alpha,b} + CN_{\alpha,f})_g - (CN_{\alpha,b} + CN_{\alpha,f})_s}{(CN_{\alpha,b} + CN_{\alpha,f})_s} \tag{4}$$

The correction for the grooves effect on the fin (in the presence of a body) can be deduced when we define F_f as

$$F_f = \frac{\Delta CN_{\alpha,f}}{CN_{\alpha,bf,s}} \equiv \frac{(CN_{\alpha,fg} - CN_{\alpha,fs})}{(CN_{\alpha,b} + CN_{\alpha,f})_s} \tag{5}$$

Therefore, because tests for body groove effects on fin lift can only be made in presence of bodies, the pure fin alone is not applicable. However, the effect of grooves on fin lift (in the presence of a body), F_f, can be deduced from both F_b and F_{bf}, after simple algebraic simplification as

$$F_{bf} = F_b\left[\frac{(CN_{\alpha,b})_s}{(CN_{\alpha,b} + CN_{\alpha,f})_s}\right] + F_f \tag{6}$$

thus,

$$F_f = F_{bf} - F_b\left[\frac{(CN_{\alpha,b})_s}{(CN_{\alpha,b} + CN_{\alpha,f})_s}\right] \tag{7}$$

Therefore, the effort in this work is to determine the values of F_b and F_{bf} from the test data, then deduce F_f. The user for any application can then use the computed values of F_b, F_f, and F_{bf} to compute $\Delta CN_{\alpha,bg}$, $\Delta CN_{\alpha,fg}$, and $\Delta CN_{\alpha,bf,g}$ based on the smooth-body values of $CN_{\alpha,bs}$, $CN_{\alpha,fs}$, and $CN_{\alpha,bfs}$. Note that the definitions of F are presented as fractions of the change in grooves lift (increase or decrease) relative to the lift value of the smooth body. The value of F_b, F_f, or F_{bf} is usually less than 0.15, indicating a 15% maximum change over the corresponding smooth-body value. As will be shown later, F_b is always positive and F_f is always negative, resulting in F_{bf} being either positive or negative, as can be implied from Eq. (6).

For most KE projectiles, the grooves are manufactured with a standard pitch-to-height ratio. Therefore, either the pitch or the groove depth may be specified. For practical aspects, the groove pitch is more visible and easily identified. Therefore, in the present work, only the grooves pitch will be reflected into the correlations. Considerably deep, nonstandard grooves may then require different considerations.

It is reported[3–5] that the location of center of pressure for body-alone and body with fins will also be slightly affected by the grooves. However, a separate study may be dedicated to investigate the exact trend and magnitude. The present work does not include this aspect. However, from the available published data, it seems that for body-alone, the center of pressure moves slightly backward, away from the nose. For finned bodies, the loss in fin lift causes a slight forward movement toward the nose. For the combined body and fins, the final shift can be forward or backward, depending on the relative contributions of changes due to the body-alone and the fins.

Body-Alone

The body-alone normal force grooves correction increment F_b was identified to be affected by the nose shape, nose length, grooved-body length, grooves starting distance from the nose end, grooves pitch, and Mach and Reynolds numbers. The associated symbols and nomenclature used are defined in Fig. 2. The following form was then assembled based on the basic factors and their contributions. This particular form was also guided by all of the data[3–5] examined. Thus,

$$\frac{\Delta CN_{\alpha,b}}{CN_{\alpha,bs}} = F_b = +0.015[F_1 \quad F_2 \quad F_3 \quad F_4 \quad F_5] \tag{8}$$

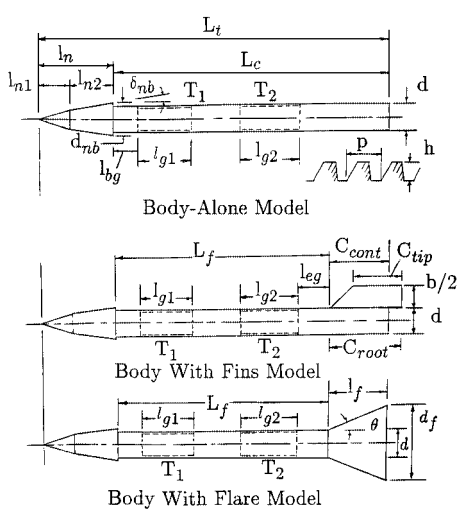

Fig. 2 Nomenclature for the present correlations.

where

$$F_1 = \left\{\left[\frac{l_n \tan^{-1}(d_{nb}/l_n)}{(l_{n1}\tau_1 + l_{n2}\tau_2)}\right]^{2.0}\left[1 + 0.1\left(\frac{L_t}{l_n}\right)^{0.5}\right]\right\}$$

$$F_2 = \left\{1 + 15.0\left(\frac{d_{nb} - d}{d}\right)[1 + 20.0\tan(\delta_{nb})]\left(1 - \frac{l_{bg}}{L_c}\right)^{4.0}\right\}$$

$$F_3 = \left\{1.165(1 - e^{-0.5 l_g/d})\left[1 + 0.15\left(\frac{l_g}{d}\right)^{0.4}\right]\left(1 - \frac{l_{bg}}{L_c}\right)\right\}$$

$$F_4 = \left\{1 + 0.28\left[\left(\frac{p_1}{0.031}\right)^{0.7}\left(\frac{l_{g1}}{L_c}\right) + \left(\frac{p_2}{0.031}\right)^{0.7}\left(\frac{l_{g2}}{L_c}\right)\right]\right\}$$

$$F_5 = \left\{\left[0.5 + 0.5\sqrt{\left(\frac{1.4 \times 10^6}{Re}\right)}\right]\left(\frac{4.0}{M_\infty}\right)^{0.2}\right\}$$

$$l_g = l_{g1} + l_{g2}$$

where p_1 and p_2 are the grooves pitch in inches and τ_1 and τ_2 are the average cone half-angles (in radians) for the first and second nose sections, if applicable. For a continuous nose surface, τ_1 and τ_2 represent the average nose slope angles at $\frac{1}{3}$ and $\frac{2}{3}$ of the nose length.

Fin in the Presence of Body

To formulate a correlation for F_f, the numerical data values from experiments had to be deduced from those of the total vehicle value represented by F_{bf} and then subtracting the body-alone contribution F_b, as indicated by Eq. (7). The values for the F_f and their trends were then used to guide the development of the correlation. The associated nomenclature is defined and shown in Fig. 2. Last, the following form was assembled, guided by the numerical values deduced from all of the data[4,5] examined:

$$\frac{\Delta CN_{\alpha,f}}{CN_{\alpha,bf,s}} = F_f = -0.09[G_1 \quad G_2 \quad G_3 \quad G_4 \quad G_5] \tag{9}$$

where

$$G_1 = \left\{\left(\frac{\delta}{0.5b}\right)\left[\frac{C_{\text{cont}}(1 + T_r)}{(d + 0.5b)}\right]\sqrt{\frac{N}{4}}\right\}$$

$$G_2 = \left\{1 + 0.1\left[\left(\frac{p_1}{0.031}\right)^{0.8}\frac{l_{g1}}{L_f} + \left(\frac{p_2}{0.031}\right)^{0.8}\frac{l_{g2}}{L_f}\right]\right\}$$

$$G_3 = \left\{1 + 0.15\left[\left(\frac{p_1}{0.031}\right)^{n1}\frac{l_{g1}}{L_f} + \left(\frac{p_2}{0.031}\right)^{n2}\frac{l_{g2}}{L_f}\right] - \left(1.4\frac{l_{eg}}{L_f}\right)\right\}$$

$$G_4 = \left\{\sqrt{\frac{Re}{5.0 \times 10^6}}\left(\frac{1}{M_\infty^{0.65}}\right)\right\}, \qquad G_5 = \{G_{\text{orien}}\}$$

$$\delta = \left(0.5 C_{f\infty} x_f \left\{\frac{0.558}{\sqrt{c_f}\left[1 - \left(2\sqrt{c_f}/0.558\right)\right]}\right\}\right)$$

$$c_f = \frac{0.558 C_{f\infty}}{0.558 + 2.0\sqrt{C_{f\infty}}}, \qquad \frac{0.242}{C_{f\infty}} = \log_{10}(R_\infty C_{f\infty})$$

$$n1 = 1 - 0.08\left(\frac{p_1}{0.031}\right), \qquad n2 = 1 - 0.08\left(\frac{p_2}{0.031}\right)$$

where N is the number of fins, δ is the compressible, turbulent, flat-plate boundary-layer thickness[11] estimated at the fin's most forward point at the root chord x_f, and T_r is the fin taper ratio ($=C_{\text{tip}}/C_{\text{root}}$).

Fin Roll Orientation Model

The roll orientation effect of the fins was reported[5] in a wind-tunnel test for four-fin configurations. The effect was large for that configuration, but is expected to be smaller for six-finned or N-finned bodies due to the smaller angular interval. The orientation factor was constructed based on the data of Ref. 5 for four fins at two roll angles. It is also constructed to yield the value of 1.0 for a six-fin configuration at zero roll angle. The fin orientation factor, in association with G_5 of Eq. (9), is formed as

$$G_{\text{orien}} = \frac{\left(N_{eff}\left\{N_i \cos^2[(\pi/N) - k]\right\}\right)}{\left[N\sum_{i=1}^{N}\cos^2(\phi_i)\right]} \tag{10}$$

where

N_{eff} = $N - 1 - \cos(N\Phi)$
Φ = configuration roll angle measured from the vertical plane ($\Phi = 0$ when the top fin is aligned with the vertical plane)
ϕ_i = individual fin panel angle plane with respect to the horizontal plane
N_i = N_{eff} (for $N = 4$), $= N$ (for $N \neq 4$)
k = $\pi/2$ (for $N = 2$), $= 0$ (for $N \neq 2$)

For a four-fin projectile at 45-deg roll, the G_{orien} is 1.0, whereas it is only 0.25 for 0-deg roll. For a six-fin vehicle with one fin alinged with the vertical plane ($\Phi = 0.0$), $G_{\text{orien}} = 1.0$, and it equals 1.5 when the roll angle Φ is 15 deg. Therefore, the fin roll orientation has, relatively, large effect on the fin lift loss due to the grooves. This effect is also more pronounced for the four-fin than that for the six-fin configurations.

Body with Fins

Let us define the grooved correction factor for body with fins. The smooth-body normal force component buildup, for no wing cant angle, is written as [Eq. (1)]

$$CN_{bf,s} = CN_{b,s} + \left(K_{w(b)} + K_{b(w)}\right)CN_{ff,s}$$

Now for a grooved body, the present analysis for the correction expression is written as

$$CN_{bf,g} = CN_{b,s}(1 + F_b) + \left(K_{w(b)} + K_{b(w)}\right)(1 + F_f)CN_{ff,s} \tag{11}$$

Note that the $(1 + F_f)$ factor appears outside both $K_{w(b)}$ and $K_{b(w)}$ because F_f was deduced by subtracting the body-alone normal force from the total vehicle value; thus, the effect of the $K_{b(w)}$ could not be separated from $K_{w(b)}$. Thus, for body with fins, combining Eqs. (4) and (6) yields

$$\frac{\Delta CN_{\alpha,bf}}{CN_{\alpha,bf,s}} = F_{bf} = F_b\left[\frac{(CN_{\alpha,b})_s}{(CN_{\alpha,b} + CN_{\alpha,f})_s}\right] + F_f \tag{12}$$

Body with Flare

For flared bodies, some limited data exist for body-alone and the body with flare.[5] The present analysis deals with the flare as if it were fins; thus, one can easily establish

$$F_{bfl} = F_b\left[\frac{(CN_{\alpha,b})_s}{(CN_{\alpha,bfl})_s}\right] + F_{fl} \tag{13}$$

To obtain the flare-in-the-presence-of-body factor F_{fl} the body-alone contribution has to be subtracted from the total vehicle (body and flare) value, as was done in the finned-body case. The body-alone is extended to the end of the flare base. From Eq. (13), one obtains

$$F_{fl} = F_{bfl} - F_b\left[\frac{(CN_{\alpha,b})_s}{(CN_{\alpha,bfl})_s}\right]$$

The experimentally deduced values for F_{fl} were then fitted into the correlation

$$\frac{\Delta CN_{\alpha,fl}}{CN_{\alpha,bfl,s}} = F_{fl} = +0.35[H_1 \quad H_2 \quad H_3] \tag{14}$$

where

$$\Delta CN_{\alpha,fl} = (CN_{\alpha,fl,g} - CN_{\alpha,fl,s})$$

As in the fin case, F_{fl} is not a purely flare-alone value, but rather flare-in-the-presence-of-body. Its definition is purely mathematical to be consistent with the body-alone and the total vehicle (body and flare) definitions. Its value is not measured directly, but rather deduced by subtracting the body-alone from the total vehicle value.

The following forms for the different H factors of Eq. (14) were formulated reflecting the given considerations and with the different constants being guided by the data set of Ref. 5. The associated nomenclature is also defined in Fig. 2:

$$H_1 = \left\{\left(\frac{\mathrm{d}_f}{\mathrm{d}}\right)\left(\frac{\mathrm{d}_f - \mathrm{d}}{2l_f}\right)\right\}$$

$$H_2 = \left\{0.3 + 0.25\left[\left(\frac{p_1}{0.031}\right)^{m1}\left(\frac{l_{g1}}{L_f}\right)\left(\frac{p_1}{0.157}\right)^{0.5} + \left(\frac{p_2}{0.031}\right)^{m2}\left(\frac{l_{g2}}{L_f}\right)\left(\frac{p_2}{0.157}\right)^{0.5}\right]\right\}$$

$$m1 = 1 - 0.05\left(\frac{p_1}{0.031}\right), \qquad m2 = 1 - 0.05\left(\frac{p_2}{0.031}\right)$$

$$H_3 = \left\{\left(0.5 + 0.5\sqrt{\frac{1.4 \times 10.6}{Re}}\right)\left(\frac{1}{M^{0.1}}\right)\right\}$$

Applying the Correlations

Equations (8), (9), (12), and (14) provide the incremental change in normal force slope coefficient due to grooves, ΔCN_α, as a fraction of the corresponding smooth-body value. This grooves correction is then added to correct the estimated normal force for the smooth-body vehicle.

Because the present correlations are based on test data, the present correlations are expected to provide best results when applied within the ranges of the parameters used. Thus, best results are obtained in the Mach range between 2.0 and 5.5, small angles of attack up to 6 deg, and to fin aspect ratios of 0.3–2.0. Results obtained by applying the correlations in regions beyond these limits should be well examined. In addition, the flare correlation was based on limited data, and thus is expected to be less versatile.

About the Data Used

Data of Khan and Chung[3]

The data of Khan and Chung[3] concern body-alone only. Four long bodies with slightly different nose shapes were tested in a blow-down wind tunnel at Mach = 4. Two different groove lengths were tested for each nose shape, in addition to the smooth-body model. The groove lengths are 3.9 and 18.5 calibers, and they both begin immediately after the nose section. All models had an L/d of about 21.8 with a model diameter of 0.77 in. Three series of body models were tested. Model series 1000 has the grooves over the total cylindrical body length, for four nose types (models 1100, 1200, 1400, and 1500). The second model, series 2000, has grooves over only the first 3.9 calibers of the body following the same nose types (models 2100, 2200, 2400, and 2500). The third model, series 4000, has no grooves at all on the cylindrical body for the same four nose types (models 4100, 4200, 4400, and 4500). Model 1100 has a 10-deg semivertex cone nose followed by short cylindrical section. Model 1200 has a 10-deg semivertex cone followed by a short 7-deg half-angle frustum. Model 1300 has two shorter conical nose sections of half-angles of 22 and 10 deg, respectively, followed by a short cylindrical section. Model 1500 has a Sears–Haack ogive nose. The test Reynolds number was about 1.4×10^6/ft. The thread types are 0.759 in.-32UNS-2A (0.759 in. mean diameter and 32 threads/in.).

Data of Brandon and von Wahlde[4]

This set of data[4] is large and encompasses body-alone and body with fins. Both configurations were tested with smooth and grooved bodies. Tests were made at Mach 3.5, 4, and 5. Bodies with L/d ratios of 20.6, 25.6, 30.6, and 35.6 were tested. The body diameter was 0.94 in., and the Reynolds number per foot varied from $(4.0\text{–}5.6) \times 10^6$. The grooved models have two sections with different types of grooves to test the effect of groove types. The notation G/S, G/T, and G/G represents front/rear body groove types (S = smooth body, T = threads of 32 threads/in., G = grooves of 8 grooves/in.). Most of the groove effects tests were made with a shortened length of a Sears–Haack nose ogive. For the finned configurations, only one set of fins (six fins) was tested at one roll angle setting (zero roll). Tests were made between $\alpha = \pm 4$ deg. Test results were questionable for some runs due to the fast continuous α sweep measurement and to the large total length of the projectile. Models were sting mounted, causing some bending of the long rods and resulting in asymmetric CN_α variation with positive and negative α. The tabulated data in the Ref. 4 report were checked vs the plotted results, when a tabulated value was noticed to be suspect. The report stated that due to this asymmetry, data points for CN were averaged over the negative and positive α, thus contaminating the correct value. Some results were limited between $\alpha = \pm 2$ instead of ± 4 deg. In some cases, the negative α sweep points were neglected altogether. In the present study, some suspect values were tracked and corrected, from their plotted values in Ref. 4. The test model for this set of data is shown in Fig. 3.

Data of Sigal[5]

This set of data was generated only for Mach numbers 0.8 and 2.4. Only the supersonic speed data were analyzed and used in the present work because the speed range for the KE projectiles is usually between $M = 5$ and $M = 2$. The tests were run for α between ± 5 deg, at Reynolds number of 25.9×10^6/ft. The diameter of the test model is 1.57 in., and the total length is 13.5 calibers. The ogival-nose length is 3.5 calibers, and the grooved section is 8 calibers long and begins at the end of the nose section. Four types of surface roughness and grooves were tested in addition to the smooth body. All surface grooves and roughnesses have a height of 0.02 in., and all grooves had sharp rectangular profiles. The first type is a knurled surface roughness whereas the second is threaded with 25.4 threads/in. The third type is grooved with 12.7 grooves/in., and the fourth type is with grooves of 6.35 grooves/in. For the finned configuration, four trapezoidal fins of aspect ratio of 1.35 and taper ratio of 0.3 were used. The configuration was tested in the + and ×, i.e., 45-deg roll, formations. For the flared configuration, a frustum conical flare of length of 2 calibers and semicone angle of 7.1 deg was used. No estimates for the error in measurements were given.

Data of Fellows–Carberry[6] and Hendry[7]

The data of Fellows and Carberry[6] are only for body with fins, at Mach numbers of 2.0, 3.0, 4.0, and 4.9. The data were summarized and reported in Ref. 7. The configuration had six trapezoidal fins of taper ratio of 0.45 and aspect ratio of 0.37. The tests were made at zero roll (one fin aligned with the vertical plane). The test model had L/d of 16.1 and diameter of 1.73 in. Three patterns of groove lengths were tested including a large single length, two smaller unconnected lengths, and a small central length. Only the two unconnected-lengths case provided consistent behavior. The grooving is 8 grooves/in. The test model for this data is shown in Fig. 4.

This set of data was not purposefully included in deriving the correlations because an independent test was needed to examine their predictions. This set was chosen because it has the unique feature of two separated grooved sections and because the data showed larger scatter. These features would test the correlations in a harsher, nontypical case.

Error Estimation for Values Deduced from Experiments

Although the error in measurements in $CN_{\alpha,s}$ and $CN_{\alpha,g}$ might be small, the error in their relative differences represented by $\Delta CN_\alpha / CN_{\alpha s}$ is quite large, as exemplified by the following example. Let the measurement errors in $CN_{\alpha s}$ and $CN_{\alpha g}$ be $\pm 3\%$, with measured values of 4.7 and 5.0 per radian, respectively. The direct value for $\Delta CN_\alpha / CN_{\alpha s}$ would be $+6.38\%$, whereas the highest and lowest possible values would be $+12.96\%$ and $+0.18\%$, respectively. This indicates a possible error of $+103\%$ or -97% in the $\Delta CN_\alpha / CN_{\alpha s}$ value of 6.38%. Therefore, although the measurements of CN_α are within $\pm 3\%$, the corresponding error in the

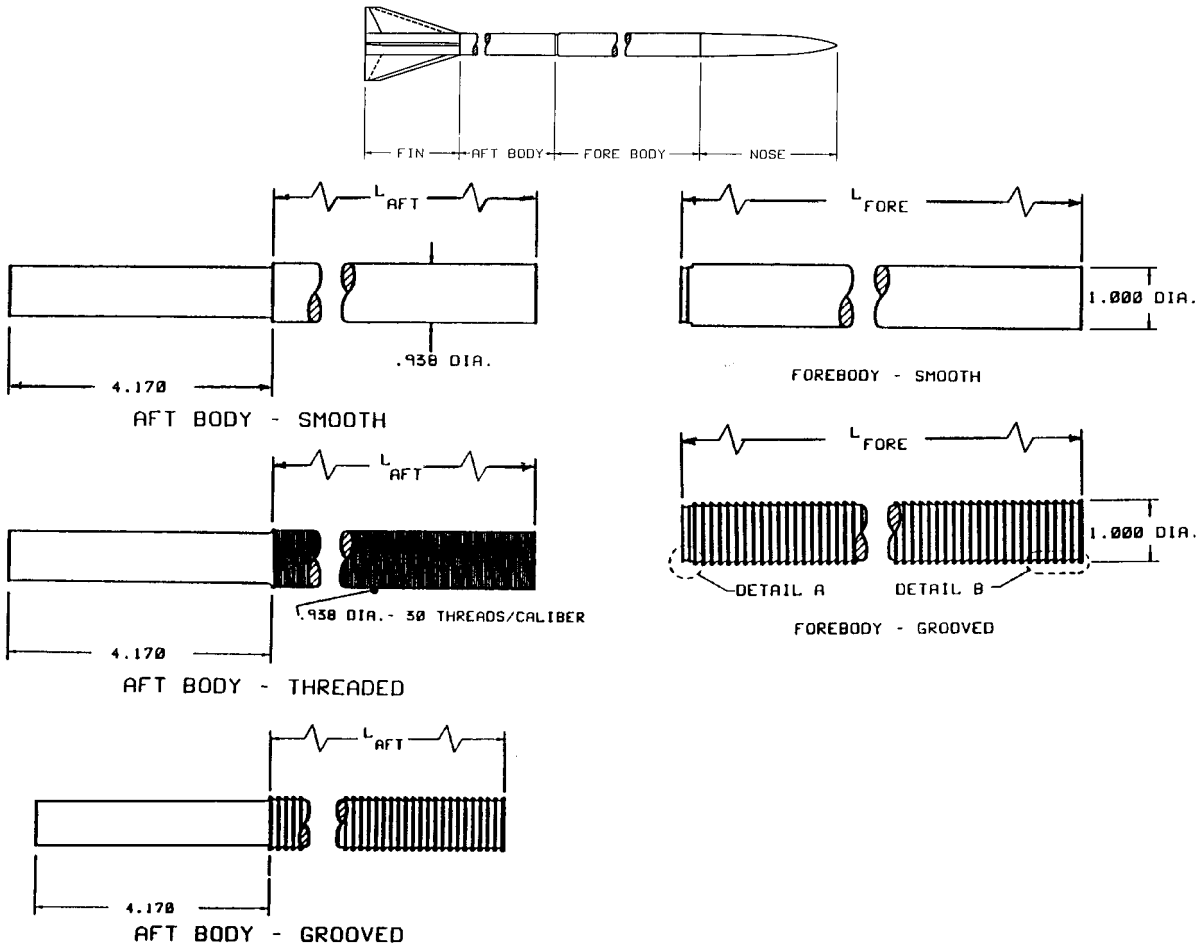

Fig. 3 Test model and grooves of Brandon and von Wahlde.[4]

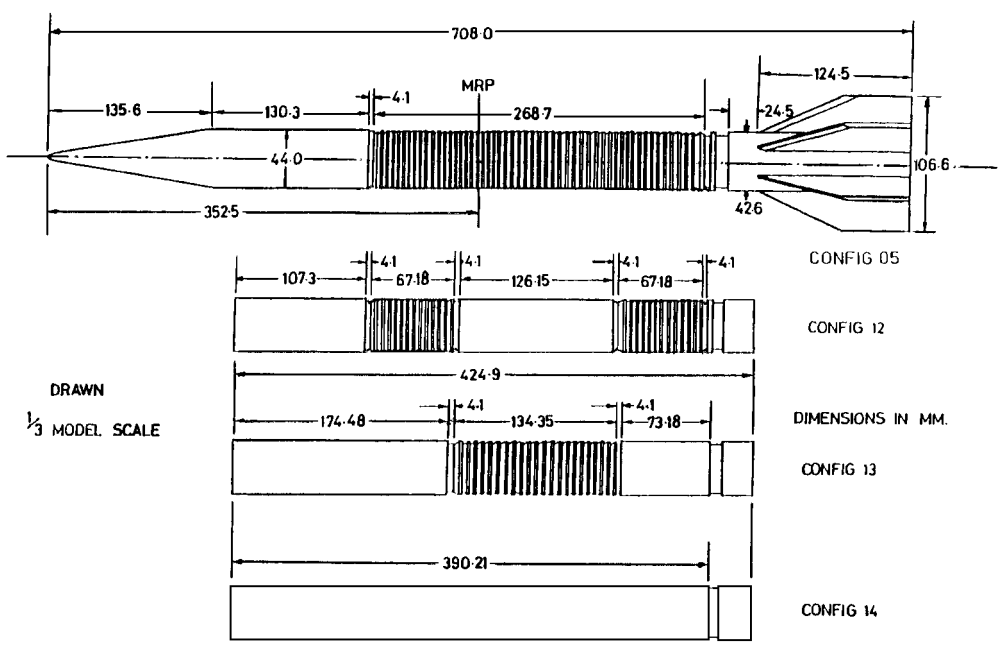

Fig. 4 Test model and grooves of Fellows and Carberry[6] and Hendry.[7] Details of various lengths of buttress thread.

deduced $\Delta CN_\alpha / CN_{\alpha s}$ is $\pm 100\%$. In the present work, the experimentally deduced values for $\Delta CN_\alpha / CN_{\alpha s}$ will be considered having an error bound of $\pm 100\%$. Thus, if the experimental F_{bf} value is -0.03, this indicates a normal force slope coefficient decrease in the range of (0.0–6.0)%.

Results

Listings of the physical parameters and the computed results for body-alone are given in Tables 1 and 2, respectively. Tables 3 and 4 provide the same for body with flare, and Tables 5 and 6 are for body with fins.

Body-Alone

Cases of Khan and Chung[3]

Figures 5–8 provide the groove effects on the body-alone of Ref. 3 For models 2100 and 4100, the increase is about +4%, as shown in Fig. 5. For models 2200 and 4200, the changes are larger and amount to +(9–14)%. For models 2400 and 4400, the changes are

Table 1 Body-alone: case designation and test conditions

Case no.	Ref.	Test model or run no.	Total length L, caliber	Length and type of grooves: l_{g1}, caliber	T_1 type (no./in.)	l_{g2}, caliber	T_2 type (no./in.)	Mach no.	Re/ft $\times 10^{-6}$
1	Khan and Chung[3]	2100	21.86	3.9	T[a] (32)	0.0	None	4.0	1.4
2		2200	21.80						
3		2400	20.94						
4		2500	21.80						
5		4100	21.86	18.6					
6		4200	21.80						
7		4400	20.94						
8		4500	21.80						
9	Brandon and von Wahlde[4]	3	20.59	6.4	G[b] (8)	4.0	T (32)	3.5	4.0
10		21					S[c]	5.0	5.6
11		24					T (32)		
12		26					G (8)		
13		4	25.59	9.6		6.0	T (32)	3.5	4.0
14		14					T (32)	4.0	4.8
15		33					S	5.0	5.6
16		39					T (32)		
17		56					G (8)		
18		59	30.58	12.4		8.0	S	5.0	5.6
19		61					T (32)		
20		62					G (8)		
21		11	35.59	15.4		10.0	T (32)	3.5	4.0
22		19					T (32)	4.0	4.8
23		72					S	5.0	5.6
24		73					T (32)		
25		74					G (8)		
26	Sigal[5]	None	13.50	8.0	K[d]	0.0	None	2.4	25.9
27					T (25.4)				
28					G_1 (12.7)				
29					G_2 (6.35)				

[a]Threaded. [b]Grooved. [c]Smooth surface. [d]Knurled.

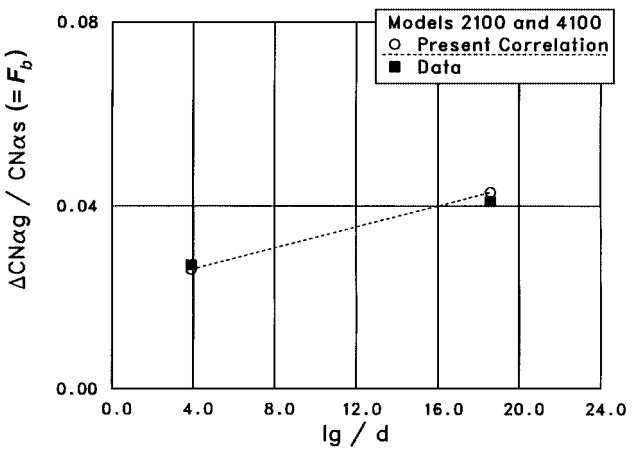

Fig. 5 Results for the body-alone of Ref. 3: M = 4, models 2100 and 4100.

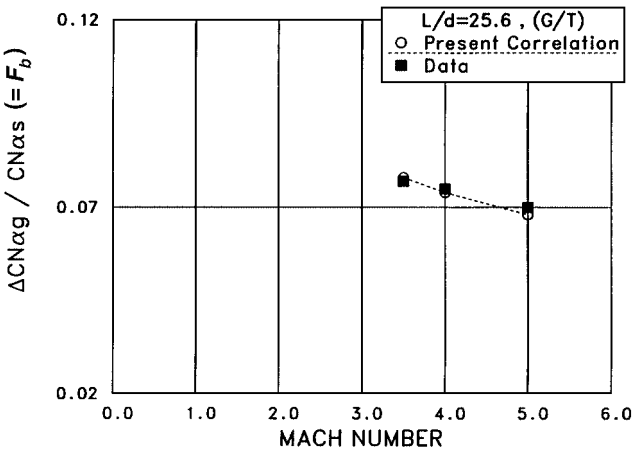

Fig. 7 Results for body-alone of Ref. 4: L/d = 25.6, G/T grooves.

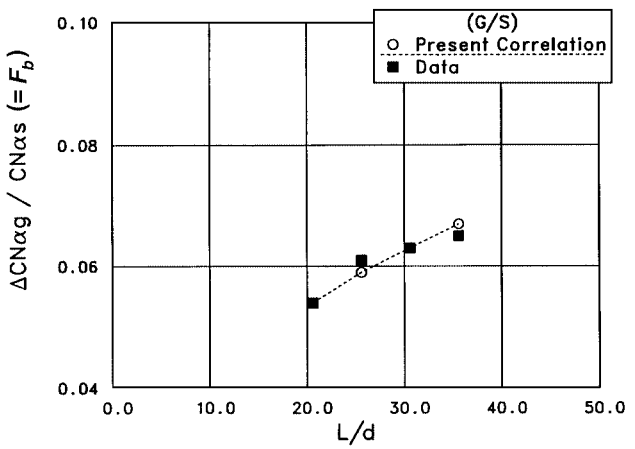

Fig. 6 Results for the body-alone of Ref. 4: M = 5, G/S grooves.

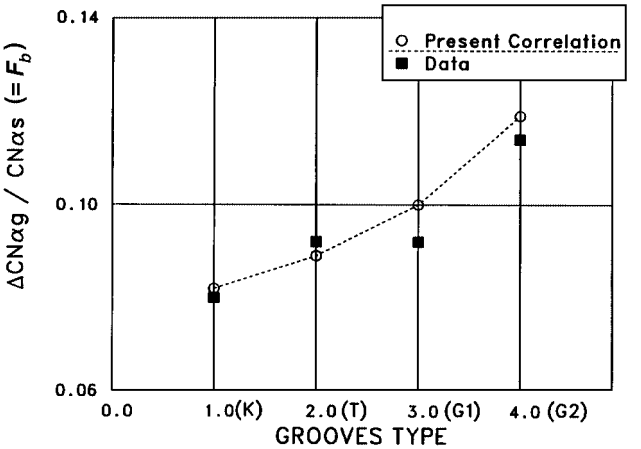

Fig. 8 Results for body-alone of Ref. 5: M = 2.4.

about +4%. Also, for models 2500 and 4500, the changes are only +5%, as listed in Table 2. The explanation for the larger values for models 2200 and 4200 is that the nose-end section has a sudden step-down junction with the body, which must have caused further flow disturbance ahead of the grooves and larger lift increase. Therefore, this step-down effect was reflected by the factor F_2 in Eq. (8).

Cases of Brandon and von Wahlde[4]

Figure 6 provides an example of the body-alone results of Brandon and von Wahlde.[4] Figure 6 provides the F_b factor at Mach = 5 for the three grooving types. The grooves increase the normal force by about +(5–8)%. The effect increases with the length of the grooves. Figure 7 shows the variation of the effect with Mach number for the body-alone. The grooves effect decreases slightly with increasing Mach number and is about +7% for the three different body lengths.

Cases of Sigal[5]

Figure 8 shows the correlation result for the wind-tunnel test of Sigal.[5] The grooves effect increased with the increased pitch of the grooves. The values increased from +8 to +12%, approximately. Note that increasing the grooves pitch is limited to about $p =$ 0.25 in., beyond which each groove tooth may act as a separate single cavity, with different flow phenomena than the present close-grooves study, as was pointed to in the Introduction.

Table 2 Body-alone: comparison with data

Case no.	CN_α, wind tunnel Grooved 1	Smooth 2	$\Delta CN_{\alpha g} =$ 1–2	$(\Delta CN_{\alpha g}/CN_{\alpha s})$ Wind tunnel	Present predictions
1	3.80[a]	3.70	+0.10	+0.027	+0.026
2	4.35	3.90	+0.45	+0.102	+0.088
3	4.05[a]	3.90	+0.15	+0.038	+0.032
4	3.90	3.75	+0.15	+0.040	+0.041
5	3.85	3.70	+0.15	+0.041	+0.043
6	4.45	3.90	+0.55	+0.141	+0.147
7	4.10	3.90	+0.20	+0.051	+0.053
8	4.00	3.75	+0.25	+0.067	+0.068
9	3.39[b]	3.19	+0.20	+0.063	+0.072
10	3.29	3.12	+0.17	+0.054	+0.054
11	3.31		+0.19	+0.061	+0.063
12	3.35		+0.22	+0.074	+0.074
13	3.81	3.54	+0.27	+0.076	+0.078
14	3.74[b]	3.48	+0.26	+0.075	+0.074
15	3.63	3.42	+0.19	+0.060	+0.059
16	3.66		+0.24	+0.070	+0.068
17	3.69		+0.27	+0.079	+0.077
18	3.87	3.64	+0.23	+0.063	+0.063
19	3.91		+0.27	+0.074	+0.073
20	3.93[b]		+0.29	+0.080	+0.082
21	4.45	4.12	+0.33	+0.080	+0.086
22	4.42	4.10	+0.32	+0.078	+0.082
23	4.33	4.07	+0.26	+0.065	+0.066
24	4.38		+0.31	+0.076	+0.076
25	4.40		+0.33	+0.081	+0.084
26	2.94	2.72	+0.22	+0.080	+0.082
27	2.97[a]		+0.25	+0.092	+0.089
28	2.99		+0.27	+0.099	+0.110
29	3.03		+0.31	+0.114	+0.119

[a]Corrected value. [b]Adjusted value due to asymmetry.

Body with Fins

Cases of Brandon and von Wahlde[4]

Reference 4 provides fewer results for body with fins than those for body-alone. The majority of tests were performed at Mach = 5 and for the $L/d = 25.6$ configuration. It was noticed that the closeness of the end of the grooves' length to the beginning of the fin forwardmost point at the fin root has a relatively large effect on the amount of loss of the fin normal force. When the second grooved section of the body (nearest to the fins) was replaced by a smooth-body section, the grooves effect on the normal force of the total vehicle was much reduced from 3.8% to about 1%, as can be seen in Fig. 9 for the G/S case. For the fully grooved body, the total vehicle lift loss was about −4%.

Cases of Sigal[5]

The results for the data of Sigal[5] for finned body at Mach 2.4 are shown in Fig. 10. What is surprising from this test is the relatively large difference in results for the fins in the + and × roll positions. In the + fin formation, only two fins are producing lift and are affected; thus, the fin lift loss contribution to the total vehicle lift is small. This small decrease in fin losses cannot outweigh the positive increase in lift attained by the body-alone, thus resulting in a net increase of the lift of the total body of about +(3–4)%. For fins in the × formation, the four fins are producing lift and are all affected by the grooves. Thus, the decrease in fin lift overcounters the increase due to the body-alone with a net decrease of about (1–2)% for the total vehicle. This example is a good application of the present analysis of the body-alone and fin-in-presence-of-body model. Through the present model, explanation for the observed results was possible.

Body with Flare: Cases of Sigal[5]

A case of body with a stabilizing conical flare was tested and presented in Ref. 5. The established correlation results for the few cases tested at Mach 2.4 are shown in Fig. 11. From the given data, the grooves are shown to cause an increase to the total vehicle lift, as was the case for the body-alone, and unlike the fin cases, which suffer a decrease in lift production. Unfortunately, there are no additional data cases to ascertain the accuracy of the predictions for other flare angles or other Mach numbers. The case of the knurled surface seems either to have been mismeasured or to have provided much smaller effect on the flare. In the prior cases for knurled surfaces for both body-alone and body with fins (Figs. 8 and 10, respectively), the knurled surface provided more consistent values as a smaller surface roughness, with regard to the magnitude of the increase in normal force. For the present case of 7-deg half-cone flare at Mach 2.4, the normal force increase varied from +6 to +14% as the groove effect increased due to the increased groove pitch.

Table 4 Body with flare: comparison with data

Case no.	CN_α wind tunnel Grooved 1	Smooth 2	$\Delta CN_{\alpha g} =$ 1–2	$(\Delta CN_{\alpha g}/CN_{\alpha s})$ Wind tunnel	Present predictions
30	4.30	4.20	+0.10	+0.024	+0.075
31	4.62		+0.40	+0.100	+0.085
32	4.73		+0.53	+0.126	+0.110
33	4.81		+0.61	+0.145	+0.144

Table 3 Body with flare: case designation and test conditions

Case no.	Ref.	Total length, L (cal)	Length and type of grooves: l_{g1}, cal	T_1 type[a]	l_{g2}, cal	T_2 type	Axial length (cal) and flare half-angle (deg)	Mach no.	Re/ft $\times 10^{-6}$
30	Sigal[5]	13.8	8.0	K	0.0	None	1.17 and 7.12	2.4	25.9
31				T (24.5 pi)					
32				G_1 (12.7 pi)					
33				G_2 (6.35 pi)					

[a]K = Knurled; T = threaded; G = grooved; and pi = (grooves) per inch.

Table 5 Body with fins: case designation and test conditions

Case no.	Ref.	Total length L, caliber	Length and type of grooves: l_{g1} caliber	T_1 type (no./in.)	l_{g2} caliber	T_2 type (no./in.)	Number, type, orientation of fins	Mach no.	Re/ft $\times 10^{-6}$
34	Brandon and	25.59	9.4	G[a] (8)	6.0	S[b]	Six fins,	5.0	5.6
35	von Wahlde[4]					T[c] (32)	clipped delta,		
36						G (8)			
37	Sigal[5]	13.5	8.0	K[d]	0.0	None	Four fins,	2.4	25.9
38				T (25.4)			clipped delta,		
39				G_1 (12.7)					
40				G_2 (6.35)					
41				K	0.0	None	Four fins,		
42				T (25.4)			clipped delta,		
43				G_1 (12.7)			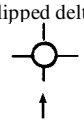		
44				G_2 (6.35)					
45	Forkois[13]	24.5	16.5	G (12.0)	0.0	None	Fin1 Four	5.44	5.5
46	(CFD)						Fin2 fins,		
47							Fin3		
48	Fellows and	16.1	1.53	G (8.0)	1.53	G (8)	Six fins,	4.9	15.5
49	Carberry[6]						clipped delta,	4.0	17.8
50	(application)							3.0	2.5
51							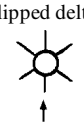	2.0	3.6

[a]Grooved. [b]Smooth surface. [c]Threaded. [d]Knurled.

Table 6 Body with fins: comparison with data

Case no.	CN_α, wind tunnel: Grooved 1	Smooth 2	$\Delta CN_{\alpha s} = 1-2$	$(\Delta CN_{\alpha g}/CN_{\alpha s})$: Wind tunnel	Present predictions
34	12.23	12.34	−0.11	−0.009	−0.013
35	11.92[a]		−0.42	−0.034	−0.039
36	11.86		−0.48	−0.039	−0.045
37	5.31[b]	5.35	−0.04	−0.007	−0.009
38	5.24		−0.11	−0.020	−0.010
39	5.25		−0.10	−0.020	−0.017
40	5.24		−0.11	−0.020	−0.020
41	5.34[b]	5.17	+0.17	+0.033	+0.030
42	5.36		+0.19	+0.037	+0.033
43	5.37		+0.20	+0.039	+0.036
44	5.40		+0.23	+0.044	+0.043
45	5.05	5.41	−0.36	−0.067	+0.015
46	5.78	6.18	−0.40	−0.064	+0.009
47	5.50	5.90	−0.40	−0.068	+0.012
48	9.00	9.20	−0.20	−0.022	−0.032
49	9.20	10.05	−0.85	−0.085	−0.052
50	11.10	11.75	−0.65	−0.055	−0.023
51	13.50	13.70	−0.20	−0.015	−0.041

[a]Adjusted value due to asymmetry. [b]Corrected value.

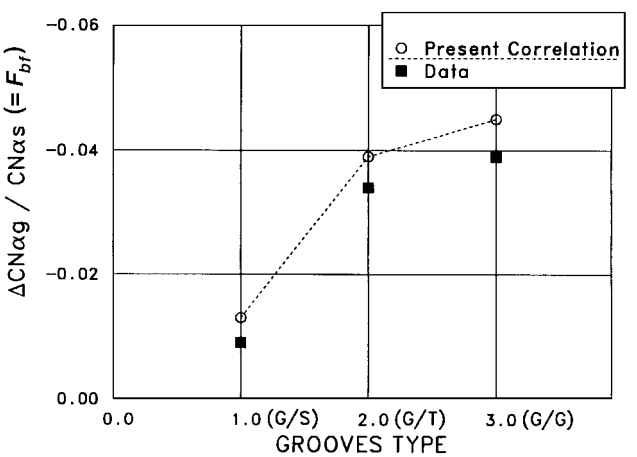

Fig. 9 Results for body with fins of Ref. 4: $M = 5$, $L/d = 25.6$, six fins.

Validation Cases of Fellows–Carberry[6] and Hendry[7]

The test data provided by Fellows and Carberry[6] and reported by Hendry[7] were not used in constructing the correlation, but were left for an independent application after the completion of the correlation. This is due to what seems to be inconsistency in data results that may be considered measurements errors, specially for these small-differences values, as explained earlier in the error estimation section.

The code of Ref. 12 was used to compute the CN_α for the smooth body-alone and body with fins for the six-fin configuration of Refs. 6 and 7, which is shown in Fig. 4. The scatter in the test data is shown in Fig. 12, which reflects the variation of F_{bf} with both Mach number and Reynolds number (see Table 5, cases 48–51, for Reynolds number). This comparison was made for the configuration having separate front- and rear-grooved sections. The other two groove configuration types showed more inconsistent results. The present correlation for body with fins provided what is believed to be well-represented effects of the total vehicle lift loss of about from −2 to −5% over the speed regime of Mach 2–5 and varying Reynolds number between (2.5 and 17.8) × 10^6/ft (Table 5, cases 48–51). The present analysis predicts the correct sign of change in lift, as well as a very reasonable magnitude of the change due to grooves.

Computational Fluid Dynamics Calculations of Forkois[13]

Computational fluid dynamics (CFD) computations were not expected to have been made for grooved bodies. The actual grooves

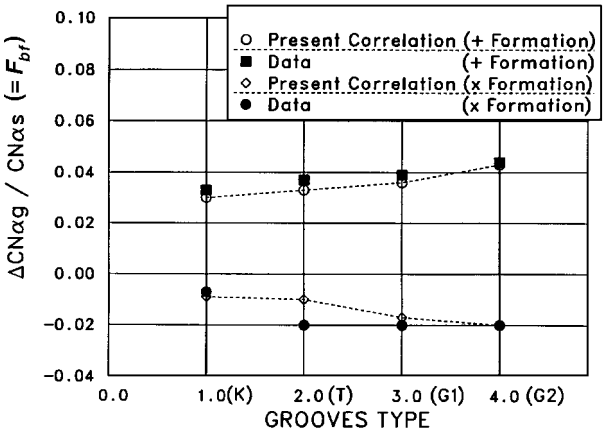

Fig. 10 Results for body with fins of Ref. 5: M = 2.4, four fins.

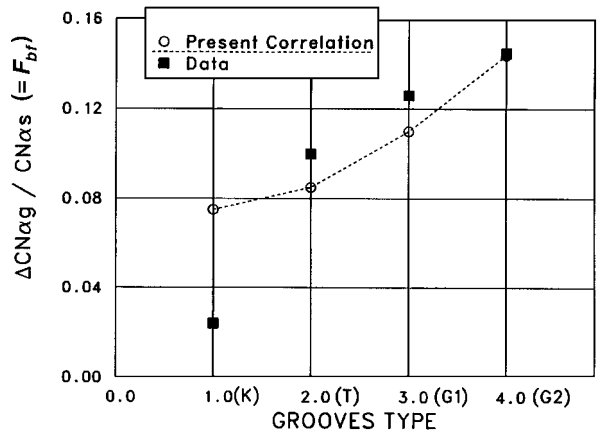

Fig. 11 Results for body with flare of Ref. 5: M = 2.4.

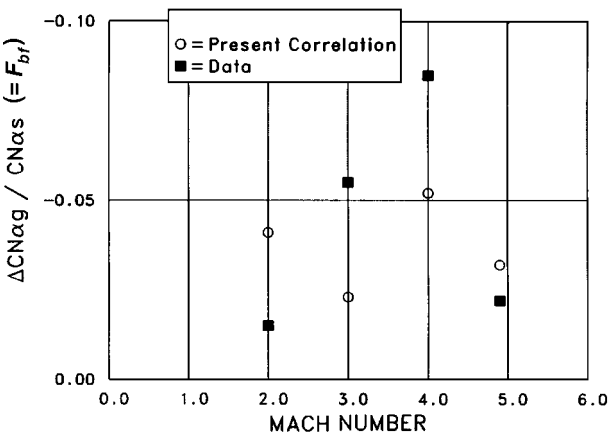

Fig. 12 Results for body with fins of Ref. 6: largely varying Reynolds number, six fins.

have sharp lines and may require a large number of grid points near each corner of each groove tooth. In addition, the smallness of the effect was thought to be uninviting for a CFD effort. However, one set of unpublished CFD calculations was reported in Ref. 13. Computations were made to investigate the suspected grooves effect on lift and the stability of a finned projectile. A parabolized Navier–Stokes code was used. Two other minor fin-shape variations were considered and computed. Only three calculations for body with the three fin shapes were computed, at Mach 5.44. For each case, computations were made for smooth and grooved body. No body-alone computations were made. Computations were made for four fins in the + formation at 1-deg angle of attack. The Reynolds number was 3.2×10^6, based on the total body length. The body diameter is 0.284 in., and the configuration is shown in Fig. 13. The actual physical grooves are 0.02 in. deep and have a pitch of 0.083 in., i.e., 12.0 grooves/in. The grooves were geometrically simplified and modeled for computation as a sinusoidal wave of depth of only

Fig. 13 Projectile configuration of Ref. 13 (with fin configuration no. 3).

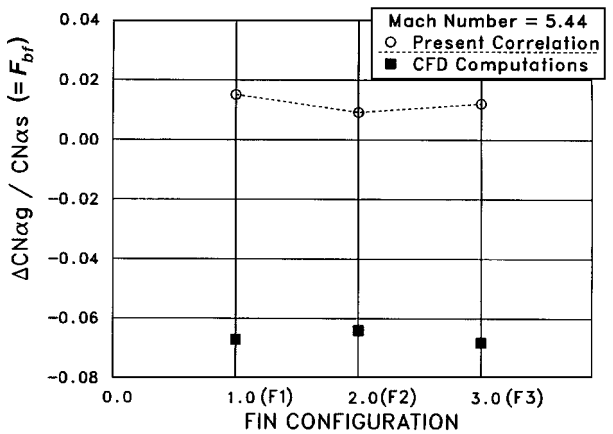

Fig. 14 Results for body with fins of Ref. 13: CFD, M = 5.44, four fins.

0.004 in., i.e., one-fifth of the actual depth, to allow continuous contoured body-surface coordinates and grids to be used. The configuration total L/d ratio is 24.5, and the grooved body length is 16.3 caliber. There are 52 grooves modeled along that length. No grid refinement studies were performed, and the grooves effects on the total normal force were, not surprisingly, almost identical for the slightly different fins.

Because of the mentioned geometrical simplifications of the grooves, the CFD computational results were not used for either establishing the correlations or validating their outcome. One might compare the results for assessing whether CFD will over- or underpredict the value. For the projectile considered, CFD predicts −6.6% (loss) in the total normal force. This value appears to be large because the normal force for this configuration is dominated by the long body and not by the small area of the only four fins. Thus, the lift increase due to the long body could not be offset by the reduction due to the small fins; therefore, it should still end up with a net increase rather than a decrease in the total normal force. The present correlation was applied, and the NSWC-AP95 code[12] was used to estimate the smooth-body values. Of the CN_α of 4.975 for the total vehicle, the long body-alone contributed 4.195 or 84.3%. The F_b, F_f, and F_{bf}, for fin configuration 2, were computed as +0.0316, −0.0175, and +0.0092, respectively. This indicates a net total increase in lift of +0.92% rather than the predicted −6.6% loss. The results are shown in Fig. 14 for the three slightly different fin shapes. It is believed that reducing the grooves depth for CFD and modeling the grooves as a continuous sinusoidal wave have significantly reduced the body-alone contribution. In addition, it is not known if a finer grid would have changed the computational outcome.

Predictive Design Example

A design example for two different KE projectile configurations is given. In the first, the total normal force will increase, whereas in the second it will decrease. It would have been surprising for a wind-tunnel test of both models (under the same flow conditions) to provide such contradictory outcome. The present analysis and correlations provide the reason and the magnitude of change for both cases. This application example is an illustration of the use of the present work.

Both configurations have 1-in.-diam and 3.5-caliber sharp conical nose. A hypothetical wind-tunnel test at Mach = 5, Reynolds number of 5.0×10^6/ft, at zero fin roll angle is simulated. The first configuration has L/d of 28.0 and the second model 13.0. Both have grooves pitch of 0.125 in. (8 grooves/in.). The first projectile has a grooved length of 20.5 caliber, whereas the second has grooved

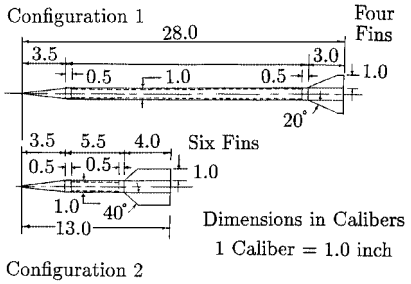

Fig. 15 Two projectile configurations of the predictive example.

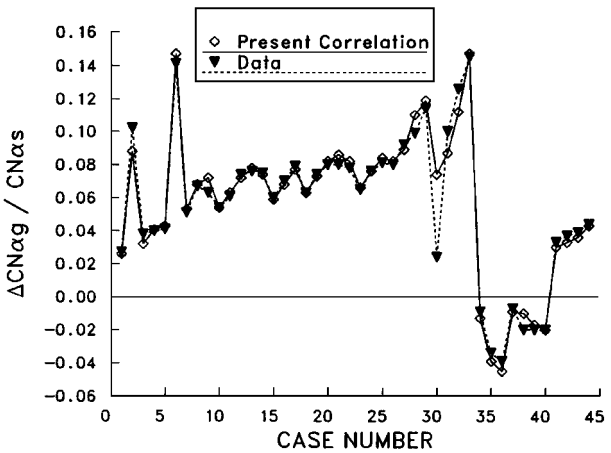

Fig. 16 Overall prediction comparison with data.

length of only 5.5 caliber. Both configurations have trapezoidal fin planforms. The first model has four small fins, with a root chord of 3.0 caliber length, whereas the second has six fins with 4.0-caliber root chord. The fin taper ratios are 0.08 and 0.70, respectively. The fin aspect ratio values are 0.36 and 0.42, respectively. The two configurations are shown in Fig. 15.

The smooth-body normal force slope coefficients were computed using the fast aerodynamics prediction code of Ref. 12. The first model has body-alone and total body CN_α of 4.29 and 6.42, respectively. The second model, similarly, has CN_α of 3.83 and 11.65, respectively. The first model has total normal force to body-alone value ratio of 1.49, whereas the second model has the value of the same ratio to be 3.04. The body-alone normal force increase factor F_b is +0.074 and +0.042 for the first and second models, respectively. The fin correction factor F_f is −0.013 and −0.049 for the first and second models, respectively. The total normal force change factor F_{bf} is +0.036 and −0.035 for the first and second models, respectively. Therefore, a wind-tunnel test would have shown a change in lift of +3.6% for the first model and a change of −3.5% for the second model, over the corresponding smooth-body values. These wind-tunnel test results would have been misinterpreted as inconsistent or contradictory. The present work not only explains these results but also quantifys the effect.

Finally, the results of the present correlations and the experimental data on which they were based, are shown in Fig. 16 for 44 cases, reflecting good agreement.

Conclusions and Summary

Based on the experimental data analyzed and the empirical correlations that were constructed reflecting them, the following conclusions are drawn for supersonic speeds and small angles of attack faced by most antiarmor projectiles: 1) An empirical model for KE projectiles based on experimental data for different shapes, fins, and speeds was developed and yielded fast, accurate predictions for the incremental lift due to surface grooves. 2) For body-alone, body grooves always result in increasing the body normal force over the corresponding smooth-body value. The largest increase observed was about +15%. 3) Body surface grooves always decrease the fin-in-presence-of-body normal force from the corresponding smooth-body value. 4) Body–fin combination may have higher or lower total vehicle normal force relative to the smooth-body value, depending on the relative length of the body, the grooved-section length, and the size and number of fins. The largest lift loss observed in this study was about −5%. 5) For body with flare, the grooves tend to increase the normal force, as if the flare was just an extension of the body-alone. The largest value observed was about +15% over the smooth-body value. 6) The location of the grooves on body-alone does not seem to be an influential factor. For the body-alone, a short grooved section of the body located after the nose caused almost the same lift increase percentage as if the whole body was grooved. 7) The grooves effect on normal force decreases with increasing flow Mach number. This effect is for both body-alone and fin-in-the-presence-of-body, and thus for the total vehicle. 8) The fin roll orientation angle has, surprisingly, a relatively large influence on the fin lift loss for cruciform fins. This effect is predicted to be less for six-fin configurations (or, generally, fin number larger than four). 9) CFD computations for a shallow wavy wall (replacing the sharp and deeper actual grooves), tend to overpredict the effect of grooves on the finned-body total normal force. For the case studied, CFD predicts −6.6% normal force decrease, whereas the present correlations provide +0.9% increase for this case of small four fins, long body, and high Mach number.

In summary, the present work provides a fast, simple method to estimate the incremental change in the normal force slope coefficient (and, thus, the normal force coefficient) for body-alone and body with fins, due to standard (i.e., typical) grooves on the projectile body. The method is based on empirical correlations, which are based on experimental data.

For future studies, a similar fast method may be established to determine the corresponding change in location of the center of pressure for the body-alone and body with fins due to grooves.

References

[1]Mikhail, A. G., "Drag Correlation and Prediction of Surface Groove Drag for Kinetic Energy Projectile," *Journal of Spacecraft and Rockets*, Vol. 26, No. 5, 1989, pp. 308–313; also AIAA Paper 88-2541, June 1988.

[2]Dupuis, A. D., "Free Flight of a Dart Model with Various Surface Roughnesses," *Proceedings of the ADPA 12th International Symposium on Ballistics*, Vol. 2, American Defense Preparedness Association, Arlington, VA, 1990, pp. 287–296.

[3]Khan, S. D., and Chung, S. K., "Effect of Geometric Variations on the Supersonic Aerodynamic Characteristics of the 75 mm XM855 APFSDS-T Projectile," U.S. Army Armament Research and Development Center, ARLCD-TR-83058, Dover, NJ, July 1984.

[4]Brandon, F., and von Wahlde, R., "Wind Tunnel Data for Long-Rod Fin-Stabilized Projectiles," U.S. Army Ballistic Research Lab., BRL-MR-3618, Aberdeen Proving Ground, MD, July 1987.

[5]Sigal, A., "Aerodynamic Effects of Body Roughness," AIAA Paper 90-2850, Aug. 1990.

[6]Fellows, K. A., and Carberry, J., "Results of Supersonic Wind Tunnel Tests on the Third Long APDS Projectile with Various Fin Designs and Buttress Threads over the Mach Number Range 2.0 to 4.9," Aircraft Research Association, Test Note M49/14, Swerby, England, UK, Feb. 1982.

[7]Hendry, C. E., "Aerodynamics of Long Projectiles—Final Report, Part 2," British Aerospace PLC, Dynamics Group, Rept. JS 10134, Swerby Research Center, Bristol, England, UK, Aug. 1984.

[8]Dupuis, A. D., "Aerodynamic Characteristics of a Dart Model with Various Surface Roughness from Free-Flight Tests," Defence Research Establishment, DREV M-2956/89, Valcartier, PQ, Canada, Jan. 1989.

[9]Abate, G., Hathaway, W., and Whyte, R., "ARF-Alliant Test Program: Aerodynamic Results," Aeroballistic Research Facility Rept. Wright Lab., Eglin AFB, Arrow Tech Associates, Contract F08635-90-C-0038, April 1994.

[10]Babinsky, H., and Edwards, J. A., "Large Scale Roughness Influence on Turbulent Hypersonic Boundary Layers Approaching Compression Corners," *Journal of Spacecraft and Rockets*, Vol. 34, No. 1, 1997, pp. 70–75.

[11]Van Driest, E. R., "Turbulent Boundary Layer in Compressible Fluids," *Journal of the Aeronautical Sciences*, Vol. 18, No. 3, 1951, pp. 145–160.

[12]Moore, F. G., Hymer, T. C., and McInville, R. M., "The 1995 Version of the NSWCDD Aeroprediction Code: Part II—Computer Program User's Guide and Listing," Naval Surface Warfare Center–Dahlgren Division, NSWCDD/TR-95/5, Dahlgren, VA, March 1995.

[13]Forkois, J., "Cannon Caliber Electromagnetic Gun (CCEMG)," Scientific and TR (Draft), Kaman Sciences Corp., Denver, CO, for United Defense, L.P., Corp., U.S. Army Contract DAAA21-92-C-0060, 1994, pp. 1.3-197–1.3-228.

J. R. Maus
Associate Editor